ROYAL SOCIETY
OF CHEMISTRY

REVIEW

Check for updates

Structural evolution of metal single-atoms and clusters in catalysis: Which are the active sites under operative conditions?

Shiyan Wang,†[a] Chaopeng Liu,†[a] Weiyao Hao,[a] Yanling Zhuang,[a] Jianmei Chen,[a] Xianjun Zhu,[a] Longlu Wang,*[a] Xianghong Niu, [b] Jianjun Mao,*[c] Dongwei Ma [d] and Qiang Zhao [a]

The structural evolution of metal single-atoms and clusters has been recognized as the new frontier in catalytic reactions under operative conditions, playing a crucial role in key aspects of catalytic behavior, including activity, selectivity, stability, and atomic efficiency as well as precise tunability in heterogeneous catalysis. Accurately identifying the structural evolution of metal single-atoms and clusters during real reactions is essential for addressing fundamental issues such as active sites, metal–support interactions, deactivation mechanisms, and thereby guiding the design and fabrication of high-performance single-atom and cluster catalysts. However, how to evaluate the dynamic structural evolution of metal species during catalytic reactions is still lacking, hindering their industrial applications. In this review, we discuss the behaviors of dynamic structural evolution between metal single-atoms and clusters, explore the driving force and major factors, highlight the challenges and inherent limitations encountered, and present relevant future research trends. Overall, this review provides valuable insights that can inspire researchers to develop novel and efficient strategies for accurately identifying the structural transformations of metal single-atoms and clusters.

1 Introduction

Advancements in electron microscopy and spectroscopy techniques have enabled intensive studies of the dynamic structural evolution of metal clusters and single-atoms (SAs) under catalytic reaction conditions in heterogeneous catalysts, providing insights at the atomic and molecular levels.[1–6] Metal clusters and single-atom catalysts (SACs) have garnered significant

[a]*College of Electronic and Optical Engineering & College of Flexible Electronics (Future Technology), State Key Laboratory of Flexible Electronics, Nanjing University of Posts and Telecommunications, Nanjing 210023, China. E-mail: wanglonglu@njupt.edu.cn; iamqzhao@njupt.edu.cn*

[b]*College of Science, Nanjing University of Posts and Telecommunications, Nanjing 210023, China*

[c]*Department of Physics, Shanghai Normal University, Shanghai 200232, China. E-mail: jjmao@shnu.edu.cn*

[d]*School of Physics and Electronic Information, Huaibei Normal University, Huaibei 235000, China. E-mail: dwmachina@126.com*

† These authors contributed equally to this work.

Shiyan Wang received his PhD degree in 2022 under the supervision of Prof. Jinlan Wang at the School of Physics at Southeast University. He then joined Nanjing University of Posts and Telecommunications as an associate professor in 2022. His research interests focus on the theoretical simulation and design of low dimensional materials.

Shiyan Wang

Longlu Wang received his PhD degree in 2017 from Hunan University. He currently works at Nanjing University of Posts and Telecommunications. He was invited as reviewers for over 20 journals and has over 90 scientific publications with total citations over 6000 and H-index at 42. His current research interest is the 2D energy materials for hydrogen evolution.

Longlu Wang

attention due to their exceptional catalytic activity, showing greater potential for energy conversion and storage applications compared to traditional nanoparticle catalysts.[7–9] Recent studies have reported that metal SAs act as active sites in certain reactions, whereas clusters and nanoparticles (NPs) do not.[10–19] Other studies have found that metal clusters are more active sites than SAs and NPs.[20–24] In addition, metal SAs and clusters can undergo reversible transformation under reaction conditions of different applied potential, gas atmospheres, coordination environment, and temperature, *i.e.*, metal SAs can agglomerate to clusters, and metal clusters can also be dispersed to SAs.[25–27]

Despite extensive research on the design, synthesis, and application of SACs, their commercialization remains limited. Efforts to enhance activity and selectivity often result in compromised stability, a crucial factor impeding large-scale application.[10,28–34] The instability of SACs arises from the high surface energy of individual metal atoms, which causes them to aggregate into more stable clusters. This leads to the structural evolution of metal SAs into clusters under operational conditions.[35–37] For instance, under a negative potential, H adsorption drives dynamic structural evolution of Cu SAs agglomerations to clusters in Cu–N–C catalysts, enhancing C_2H_5OH and NH_3 production during NO_3^- and CO_2 reduction reaction (NO_3RR and CO_2RR).[38–41] Under pyrolysis conditions, the rare-earth, transition, and noble metal clusters undergo dynamic structural evolution into SAs, which are then stabilized by neighboring N-dopants. This process results in the formation of thermodynamically stable M–N–C structures.[42,43] Under different gas atmospheres, similar dynamic behavior is observed that Pt SAs stabilize in the O_2 atmosphere and can further undergo dynamic structural evolution to Pt clusters in either H_2 or a mixture of $CO + O_2$ atmosphere on alumina during CO oxidation.[44] Additionally, a notable structural transformation was observed in CeO_2 and TiO_2. Li's group developed a laser ablation method to control the structural evolution of Pt clusters into SAs on CeO_2, leading to enhanced CO oxidation efficiency.[45] Utilizing *ab initio* molecular dynamics (AIMD) simulations and a microkinetic model, Wang *et al.*[46,47] explored the dynamic behavior at metal/oxide interface. They demonstrated that, under varying temperatures and oxygen partial pressure conditions, Au SAs detach from Au clusters to catalyze CO oxidation and subsequently reintegrate into the Au clusters after the reaction. These dynamic transformations do not deactivate the catalysts but create actual active sites, promoting efficient chemical reactions. Unfortunately, it remains an open question whether the original anchoring sites for metal SAs are stable on a substrate, and if not, What is the structure of the genuine active site for this demanding chemical process? Consequently, a comprehensive assessment of structural evolution between metal SAs and clusters is crucial, as it will be instructive and potentially accelerate the development of research in this field.

In this review, we delve into the dynamic structural transformations between metal SAs and clusters under reaction conditions and explore the driving factors behind these changes. Subsequently, we discuss recent advances in the

Jianjun Mao obtained a Bachelor's degree and a Master's degree in Physics from Henan Normal University in 2013 and 2017 respectively, and a Doctoral degree from the University of Hong Kong in 2021. After graduation, he conducted postdoctoral research at the Quantum AI Laboratory of the University of Hong Kong. He became an associate professor at the School of Mathematics and Science, Shanghai Normal University in

Jianjun Mao

2024. His main research areas include catalyst design, prediction of superconductivity theories, search for high-pressure structures and two-dimensional material structures, electronic device transport based on the Non-Equilibrium Green's Function (NEGF), and computational simulations in the field of lithium-ion batteries.

Dongwei Ma received his PhD degree in 2012 from Fudan University. He joined Huaibei Normal University in 2024 and was promoted to full professor in 2023 at Henan University. His research area is energy catalysis, including the theoretical modelling and experimental design of advanced electrocatalysts for applications in fuel cell, water electrolysis, ammonia synthesis, and CO_2 reduction etc.

Dongwei Ma

Qiang Zhao received his PhD degree in 2007 from Fudan University. He then became a postdoctoral fellow at Nagoya University of Japan. He joined Nanjing University of Posts and Telecommunications in 2008 and was promoted to full professor in 2010. His research area is organic optoelectronics, including the design, synthesis, and excited-state tuning of organic semiconductors for applications in optoelectronic

Qiang Zhao

devices and biomedical fields.

aggregation of metal SAs into clusters and the reverse transformation from metal clusters into SAs. Finally, we summarize the dynamic structural transformation behaviors observed in catalytic processes, discuss the challenges and inherent limitations encountered, and present relevant future research trends. Overall, the catalytic activity is closely linked to the dynamic structural changes of metal species, as revealed through experimental and theoretical studies. Real-time and spatial monitoring of these changes is vital for uncovering the molecular-level mechanisms of catalysis, determining the structure–activity relationship, and identifying the underlying causes of catalyst deactivation.

2 Structural transformations in catalysis

2.1 Structural transformations between metal single-atoms and clusters

Based on experimental and theoretical insights, we propose a model elucidating the dynamic structural evolution between metal SAs and clusters (Fig. 1), exploring its driving factors. In Fig. 1a, the top section illustrates the movement and coalescence of clusters, resulting in the formation of larger aggregates, where atomic species migrate from smaller clusters to larger ones.[48] The agglomeration of metal SAs into clusters has been observed under operating conditions of varying catalytic reactions such as CO_2RR, NO_3RR, CO oxidation, and oxygen

reduction reaction (ORR) due to different gas atmospheres, negative potential, or as a result of changes in coordinative structures and size effects of metal species, as depicted in Fig. 1b.[38–41,44,49–51] Unlike sintering, redispersion (shown at the bottom of Fig. 1a) leads to a reduction in the size of metal species and increases the proportion of surface atoms in heterogeneous catalysts. Fig. 1b highlights the dynamic transition from metal clusters into SAs, driven by strong interactions between the donor atoms on the support and the diffusing metal atoms during different catalytic reactions. This transformation occurs through various strategies such as electrochemical knock-down, applied potential, laser irradiation, thermal treatment, and so on.[42,43,45–47,52–56]

2.2 Structural transformations of metal single-atoms into clusters

Yang et al.[57] presented a notable example of dynamic structural changes in M–N–C SACs, focusing on the potential-driven evolution of Cu–N–C during the ORR, as illustrated on the left side of Fig. 2a. Through operando XAS and density functional theory (DFT) calculations, they tracked the transition from Cu SAs with a $Cu-N_4$ coordination at 0.82 V to $Cu-N_3$ at 0.50 V vs. RHE, and eventually to $HO-Cu-N_2$ at 0.10 V. These observations suggest that further reduction in potential could lead to the dissociation of Cu–N bonds, resulting in the formation of Cu clusters. In a separate study, Yang et al.[38] investigated the transformation of Cu–N–C SACs into clusters during NO_3^-
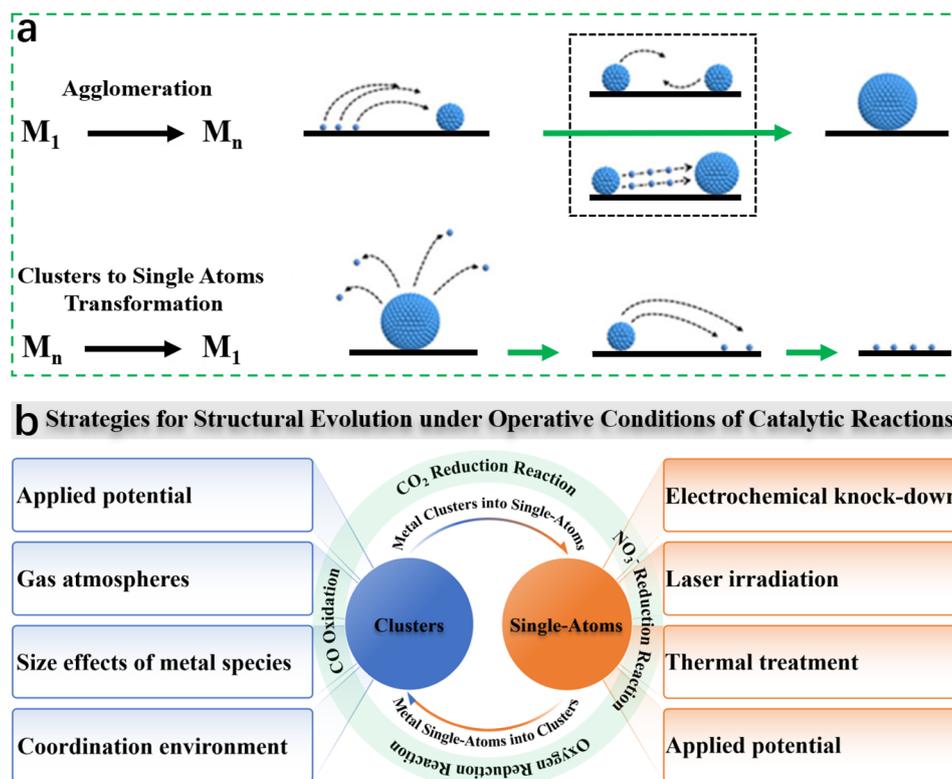

Fig. 1 (a) Schematic representation of structural evolution between metal SAs and clusters.[48] (b) Strategies for the structural evolution of metal SAs and clusters under operating conditions of different catalytic reactions.
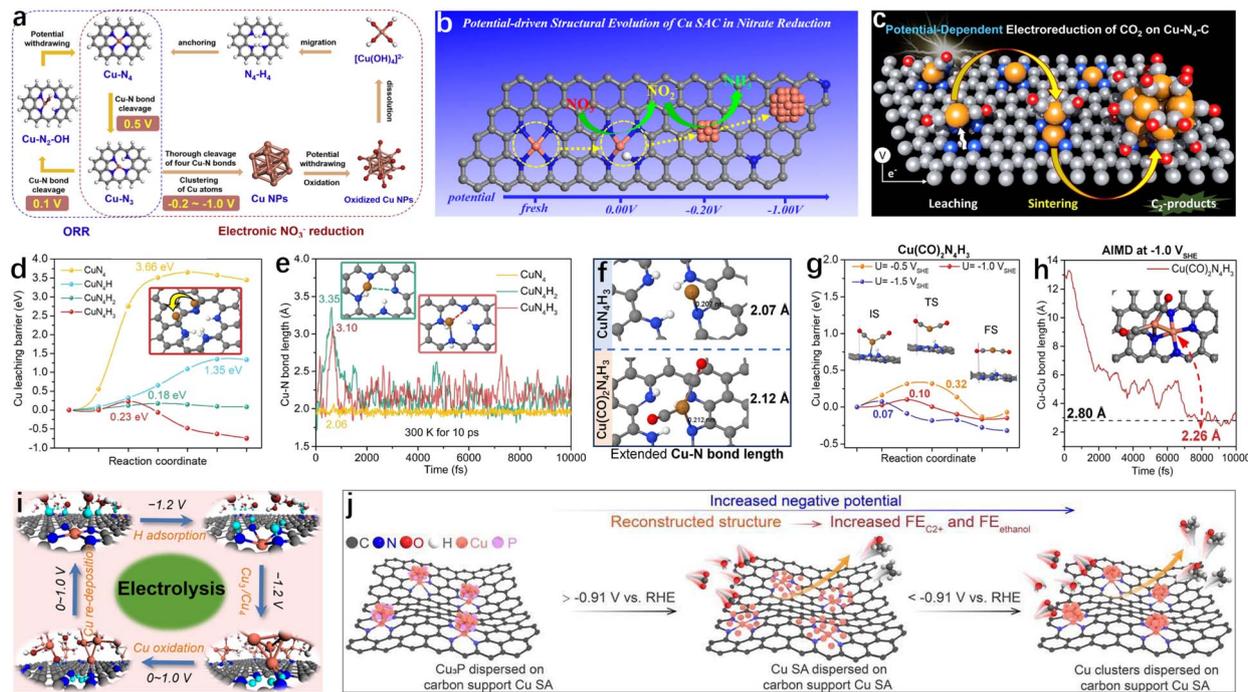
Fig. 2 (a) Schematic representation of the potential-induced structural evolution of Cu–N–C SACs during ORR and NO$_3$RR.[36] (b) The aggregation of Cu SAs into clusters is driven by the applied potential switching from 0.00 to −1.00 V vs. RHE, accompanied by NH$_3$ production.[38] (c) A novel pathway involving the evolution of Cu–(CO)$_x$ moieties driven by the synergistic adsorption of CO and H was proposed for dynamic Cu sintering in Cu–N–C catalysts under the CO$_2$RR condition. (d) The leaching barriers of Cu at −1.0 V$_{SHE}$ were determined through constant-potential CI-NEB calculations. (e) The bond lengths of Cu–N in CuN$_4$, CuN$_4$H$_2$, and CuN$_4$H$_3$ were monitored during a constant-potential AIMD simulation for 10 ps at $U = -1.0$ V$_{SHE}$. (f) The optimized structures of CuN$_4$H$_3$ and Cu(CO)$_2$N$_4$H$_3$. (g) The constant-potential Cu leaching barriers on Cu(CO)$_2$N$_4$H$_3$ at $U = -0.5$, −1.0, and −1.5 V$_{SHE}$. (h) Cu–Cu bond lengths in Cu(CO)$_2$N$_4$H$_3$ were observed during an additional 10 ps of the AIMD simulation following the leaching of the Cu–(CO)$_2$ moiety.[39] (i) The mechanism underlying the dynamic reversible transformation between Cu SAs and Cu$_4$ clusters is driven by potential-induced structural evolution.[40] (j) Schematic diagram of electrochemical reconstruction pathway of Cu$_3$P/Cu–N/C catalyst to Cu$_x$/Cu–N/C during the CO$_2$RR.[41]

reduction at potentials ranging from −0.2 to −1.0 V vs. RHE (Fig. 2a, right). Using operando EXAFS and identical-location electron microscopy, they observed this dynamic transformation, with the detailed mechanism outlined in Fig. 2b. The production rate and faradaic efficiency of NH$_3$ peaked at −1.0 V, achieving values of 4.5 mg cm^{-2} h^{-1} and 84.7%, respectively, confirming that Cu clusters act as the active species. Upon removal of the applied potential and exposure to air, the Cu clusters naturally atomized, reverting to the original Cu–N–C SACs configuration.

To confirm the existence of a genuine dynamic structural transformation behavior in Cu–N–C catalysis, constant-potential AIMD simulations have revealed that synergistic adsorption of H and CO intermediates can promote the sintering process, leading to the agglomeration of Cu SAs into clusters under CO$_2$RR conditions (Fig. 2c).[39] To better understand the kinetics of Cu sintering, the energy barriers for Cu migration from the initial N-coordinated site to a neighboring C site at −1.0 V$_{SHE}$ were calculated using potential-dependent climbing image nudged elastic band (CI-NEB) simulations. As shown in Fig. 2d, the leaching barriers for Cu migration from the N-coordinated site in CuN$_4$ to an adjacent C site decreased notably upon the adsorption of 0, 1, 2, and 3H atoms, with values dropping to 3.66, 1.35, 0.18, and 0.23 eV, respectively.

During constant-potential AIMD simulations at 300 K for 10 ps, the Cu–N bond lengths in CuN$_4$, CuN$_4$H$_2$, and CuN$_4$H$_3$ were monitored. As depicted in Fig. 2e, the Cu–N bond length in CuN$_4$ remained stable at approximately 1.9 Å, indicating the Cu atom's resistance to leaching. However, bond breaking in CuN$_4$H$_2$ and CuN$_4$H$_3$ occurred at 614 fs and 670 fs, respectively, once the bond length surpassed 2.95 Å. After bond breaking, the desorbed Cu atoms retain the ability to coordinate with adjacent H-adsorbed N atoms, thereby impeding their swift migration. Furthermore, they found that adding CO intermediate in the form of Cu–(CO)$_x$ moieties can significantly accelerate the spillover and clustering of the Cu SAs in Cu–N–C catalysts (Fig. 2f–h). This finding was further supported by theoretical calculations from Bai et al.,[40] H adsorption is crucial in driving the reversible dynamic transformation between Cu SAs and Cu$_4$ clusters by applying potential-driven structural evolution in Cu–N–C catalysis under the CO$_2$RR conditions (Fig. 2i). Experimentally, Zang et al.[41] demonstrated that the electrochemical structural evolution of Cu$_3$P particles under increasing negative potential resulted in the gradual formation of Cu clusters through dispersion and assembly (Fig. 2j). These Cu clusters exhibited an ethanol faradaic efficiency of approximately 40% and a partial current density of around 350 mA cm^{-2} during CO$_2$RR. Similar potential-driven transformations in

coordination and electronic structures, such as the transition from $M-N_4$ to coordination-unsaturated $M-N_x$, were also observed in Ni–N–C, Co–N–C, and other catalytic systems.[58–60]

Large periodic holes in g-C_3N_4 provide sufficient space, rendering it an ideal substrate for supporting catalysts.[61–65] As a result, the incorporation of metal species can significantly alter the electronic structures, with the synergistic interaction between the metal species and g-C_3N_4 playing a pivotal role in improving the catalytic performance of g-C_3N_4.[66–73] As mentioned above, Cu SAs often undergo leaching and aggregation processes into clusters during chemical reactions. Using *operando* attenuated total reflectance surface-enhanced infrared absorption spectroscopy, Zhang *et al.*[74] conducted experiments in a specialized electrochemical cell to quantitatively track the electrochemical transformation of Cu SAs into clusters on a g-C_3N_4 substrate under CO_2RR conditions, as illustrated in Fig. 3a. The reconstruction of Cu SAs is strongly influenced by the applied potential, with the rate of Cu clusters evolution at -1.2 V being roughly two orders of magnitude greater than at -0.6 V during the CO_2RR (Fig. 3b). Furthermore, DFT calculations show that the coordination environment can be adjusted by modulating the interaction between the Cu SAs and the catalyst substrates.

To evaluate the dynamic structural transformation behavior of Cu SAs to clusters on g-C_3N_4, constant-potential AIMD simulations with a slow-growth approach were performed. As shown in Fig. 3c, the Cu_1 atom of Cu_1/g-C_3N_4 can readily migrate from the original position to its adjacent equivalent position with a kinetic barrier of only 0.28 eV. Further, the AIMD simulations demonstrate that the Cu_1 can be readily aggregated into Cu_2, and then into Cu_3 and Cu_4 clusters by utilizing

available free Cu_1 species, as depicted in Fig. 3d. As we all know, the C–C coupling is crucial for C_2 products, Zhang *et al.*[75] investigated its reaction process. As illustrated in Fig. 3e, the kinetic barrier of *CO coupling significantly decreases to merely 0.41 eV when the number of atoms in the Cu clusters reaches three. Fig. 3f depicts the mechanism of activity origin of Cu species toward CO_2RR to C_{2+} products: not one, not two, but at least three atoms can efficiently promote CO–CO coupling, as determined by kinetic analyses. Similarly, Bai *et al.*[76] designed Cu_4 clusters loaded on the natural pore structure of g-C_3N_4, featuring a Cu^0–Cu^x atomic interface, for highly efficient and selective CO_2RR into C_2H_5OH.

In addition to the two-dimensional materials of M–N–C and g-C_3N_4 mentioned above, the structural transformation of metal clusters formation process has also been studied on the surfaces of transition-metal (TM),[77–79] metal oxide of ZnO_2 (ref. 49) and γ-Al_2O.[44] Yang *et al.*[77] explored the dynamic changes in composition, morphology, and structure under the CO_2RR conditions using *operando/in situ* techniques. As illustrated in Fig. 4a, monodisperse Cu undergoes a structural transformation, where the surface oxide is decreased, followed by ligand desorption, resulting in aggregated Cu clusters. These changes correlate with the generating catalytically active sites that promote higher C_{2+} formation.

The formation of active sites on the TM occurs through the surface atom's migration toward the clusters, driven by the reaction. As depicted in Fig. 4b, the adsorbate-induced cluster formation occurs in three steps: (i) step-edge atoms ejection, leading to the formation of adatoms on an adjacent terrace, (ii) diffusion of adatoms, and (iii) the adatoms aggregation to form clusters. Using DFT calculations, Xu *et al.*[78] introduced the
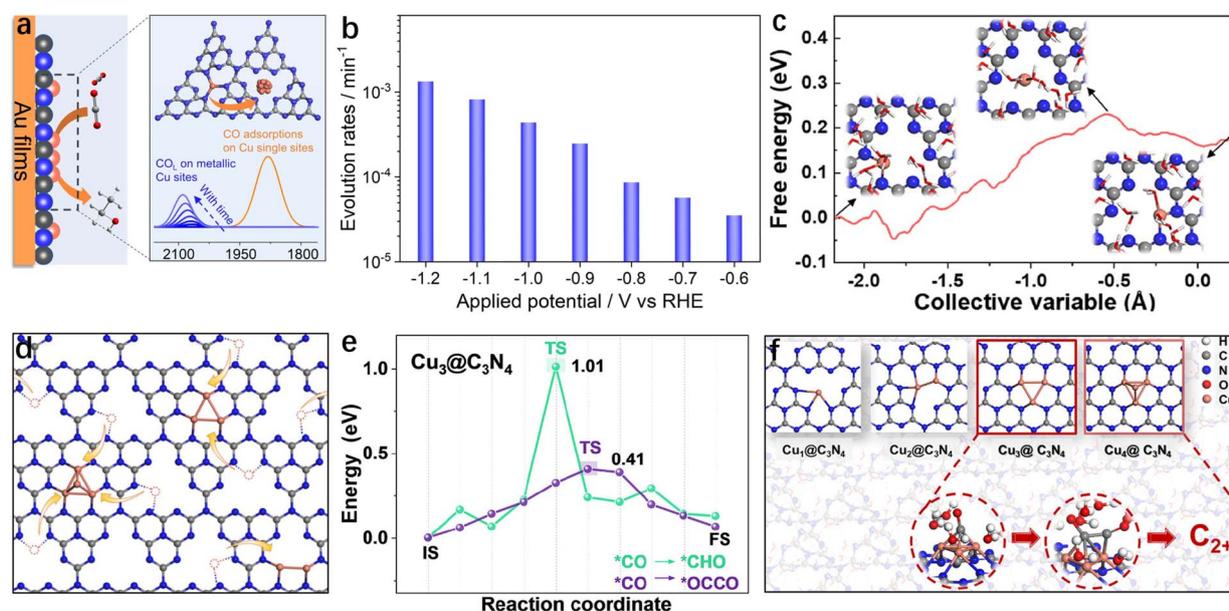

Fig. 3 (a) Schematic representation of the electrochemical reconstruction of Cu SAs to clusters on g-C_3N_4 substrate under CO_2RR condition. (b) Evolution rates of Cu single sites are dependent on the applied potential.[74] (c) Free energy diagram of original Cu SAs migrating to its adjacent equivalent position of Cu_1/g-C_3N_4. (d) Schematic of the aggregation process of Cu clusters on the Cu_1/g-C_3N_4 SACs. (e) Kinetic barriers of *CO → *CHO and *CO → *OCCO on Cu_3/g-C_3N_4. (f) Activity origin of Cu species toward CO_2 electroreduction to C_{2+} products.[75]

adatom formation energy as a descriptor for efficiently screening clustering systems. They further employed kinetic Monte Carlo simulations to investigate the CO-driven cluster formation on a Cu surface (Fig. 4c). In addition, Liu et al.[79] developed a reliable Cu–C–O machine learning force field with ab initio accuracy, enabling an in-depth understanding of the reconstruction mechanism and distribution of active sites on Cu surfaces under a CO atmosphere through state-of-the-art deep potential molecular dynamics. Combining cluster distribution statistical analysis with microkinetic simulations, they established a strategy to quantitatively evaluate the overall turnover frequency of catalyst surfaces during dynamic catalytic processes. The results indicate that edge Cu atoms undergo rearrangement, ejection, diffusion, and aggregation under a CO atmosphere, leading to the dynamic formation of cluster active sites. These small clusters in dynamic equilibrium are considered the origin of the high catalytic activity of Cu-based catalysts in low-temperature water–gas shift reactions.

EXAFS characterization revealed that during the CO_2 hydrogenation reaction, Cu atoms migrate to the surface of Cu/ZrO_2 catalysts, highlighting the impact of metal size on catalytic behavior.[49] Fig. 4d and e illustrate that varying Cu loading results in catalyst formations of different sizes, directly affecting product selectivity. At <2 wt%, the migrated Cu species did not

accumulate but remained distributed in a monodispersed state, resulting in the exclusive production of CH_3OH and a linear increase in CO_2 conversion with increasing Cu loading. When Cu loading was between 4 and 8 wt%, the migrated Cu species partially aggregated into clusters, increasing CO_2 conversion and CO selectivity, while CH_3OH selectivity decreased. Above 8 wt%, some of the Cu species aggregated to form large Cu particles that cannot activate CO_2. Though the size of active metal species remains unchanged before and after the reaction, migration, and diffusion of metal species may occur during CO_2RR process, thereby revealing the actual active sites.

Gas molecular atmosphere significantly influences the dynamic structural transformation from single metal atoms into clusters. Based on the operando XAS, DRIFTS monitoring, and STEM images, Dessal et al.[44] reported (Fig. 4f) that Pt SAs stabilize in the O_2 atmosphere and can further undergo dynamic structural transformations into Pt clusters in either H_2 or a mixture of CO + O_2 atmosphere on γ-Al_2O_3 during CO oxidation. Fig. 4g and h present a quantitative comparison of changes in white line intensities and coordination numbers (CN) of Pt–Pt. Transitioning from 0.3Pt COOX10 to 1Pt COOX10 or 0.3Pt COOX2 led to a decrease in white line intensity, indicating that increased Pt loading and reduced O_2 concentration promote Pt reduction. During the initial reaction cooling stage,
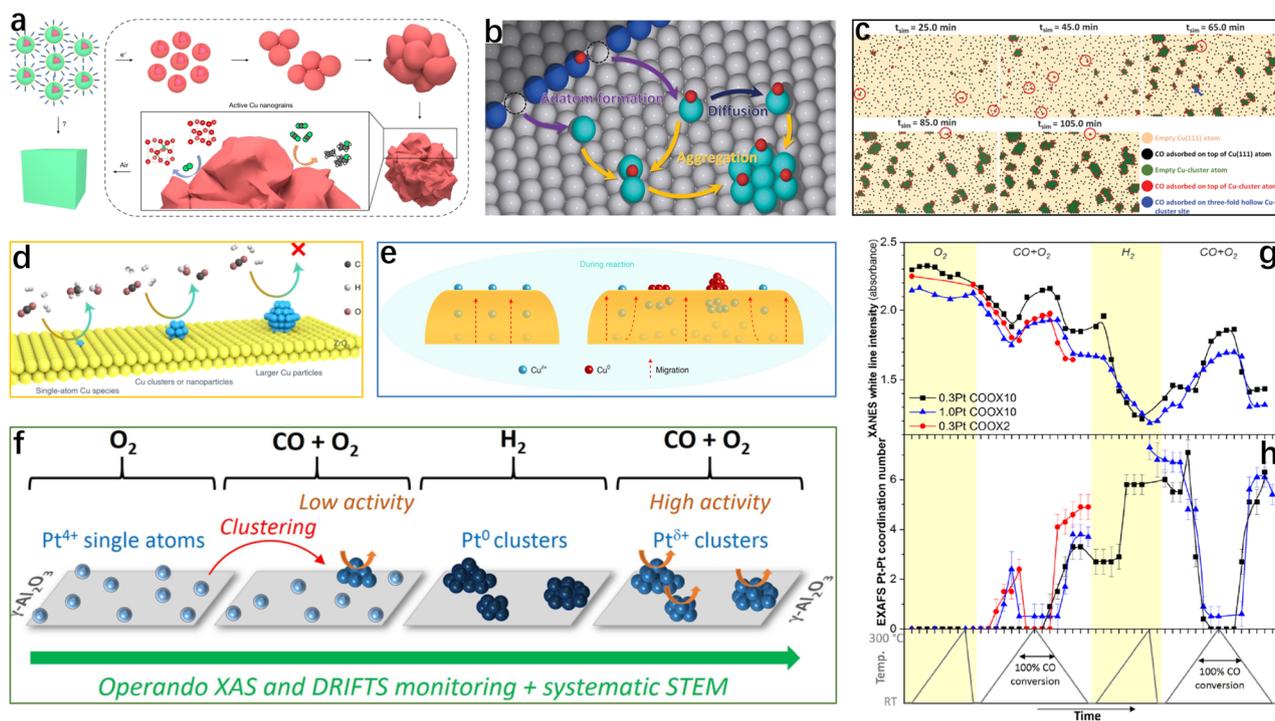

Fig. 4 (a) Monodisperse Cu NPs structural transformation to the active metallic Cu nanograins by operando/in situ methods under the CO_2RR condition.[77] (b) Schematic diagram of the catalyst structures evolution of the cluster formation on a TM surface under realistic reaction conditions.[78] (c) Snapshots from kinetic Monte Carlo simulations illustrating the evolution of a Cu(111) surface under exposure to 0.3-torr CO at room temperature, taken at intervals throughout a total simulation period of 105.0 min. (d) Schematic representation of the CO_2 hydrogenation reaction on various Cu species, highlighting their impact on product selectivity.[49] (e) Schematic illustration depicting the migration of copper species at varying Cu loadings within ZrO_2 during CO_2 hydrogenation reaction. (f) Dynamics structural evolution of Pt SAs into clusters on γ-Al_2O_3 during CO oxidation monitored by the operando XAS, DRIFTS monitoring, and STEM images.[44] (g) XANES evolution white-line intensities and (h) EXAFS analysis of Pt–Pt CN during the calcination, reaction, reduction, and subsequent reaction sequence for 0.3 wt% Pt/γ-Al_2O_3 under COOX10 and COOX2 conditions, and for 1.0 wt% Pt/γ-Al_2O_3 under COOX10 conditions.

COOX2 conditions caused a more substantial rise in CN, reaching a peak CN of 5, compared to a CN of 3–4 under COOX10 conditions. Consequently, the more reductive COOX2 environment facilitates the dynamic transformation of Pt SAs into clusters.

Significantly, to monitor the structural evolution of Cu SAs on the CeO$_2$ catalyst during C–N coupling with varying applied potential, Wei et al.[80] performed in situ XAS experiments. The Cu R-space EXAFS spectrum reveals that the coordination of the first shell of Cu transition from Cu–O to Cu–Cu bonding, i.e., Cu^{2+} is gradually reduced to Cu$^+$ and Cu^0 at the reduction potential, indicating the formation of Cu clusters. Furthermore, when the applied potential shifts to an open-circuit potential, the Cu clusters undergo a dynamic and reversible transformation back into SAs.

2.3   Structural transformations of metal clusters into single-atoms

The opposite of the above transformation behavior occurred on the metal oxide of CeO$_2$ and TiO$_2$, the M–N–C under electrochemical knock-down, applied potential, laser irradiation, and thermal treatment. Since the concept of "SACs" was first proposed by Zhang et al.[81] in 2011, SAs attracted increasing attention from researchers due to their remarkable catalytic activity compared with NPs or clusters, which is attributed to their 100% atomic utilization. Fu et al.[45] presented a laser-induced mechanism, as shown in Fig. 5a, to precisely regulate the dynamic transformation of Pt clusters into SAs on CeO$_2$. The chemical potential of Pt across varying oxygen chemical potentials, illustrated in Fig. 5b, provides insights into the configuration of the active center. The configuration identified as the most stable, Pt–O$_v$–Ce$_v$-d ionic platinum, contains one cerium vacancy (Ce$_v$) and one oxygen vacancy (O$_v$) with a chemical potential of −0.50 eV. This low energy level indicates that Pt clusters could disperse spontaneously if the leaching barrier is overcome through thermal or laser activation.

Fig. 5c presents a schematic illustration of the dynamic behavior at the metal/oxide interface, outlining the following catalytic steps: (i) CO adsorption initiates the formation of isolated Au–CO, which interacts with lattice oxygen ions, producing a CO$_2$ molecule; (ii) Au SAs then reassemble into clusters; (iii) a subsequent CO adsorption generates another isolated Au–CO complex; (iv) O$_2$ adsorbs at the O$_v$ site, and the second CO molecule reacts with this adsorbed O$_2$, resulting in an additional CO$_2$ molecule. Based on AIMD simulations, they also performed the dynamics and structural transformations of Au clusters to SAs on CeO$_2$. In the absence of CO adsorption, a 14 ps AIMD simulation confirmed that creating an isolated Au atom is energetically unfavorable. In contrast, in the presence of CO, the dynamics structural evolution of Au clusters required only 2 ps to SAs, where CO was initially located at a low-coordination interfacial Au site (Fig. 5d).[46] In a separate study,
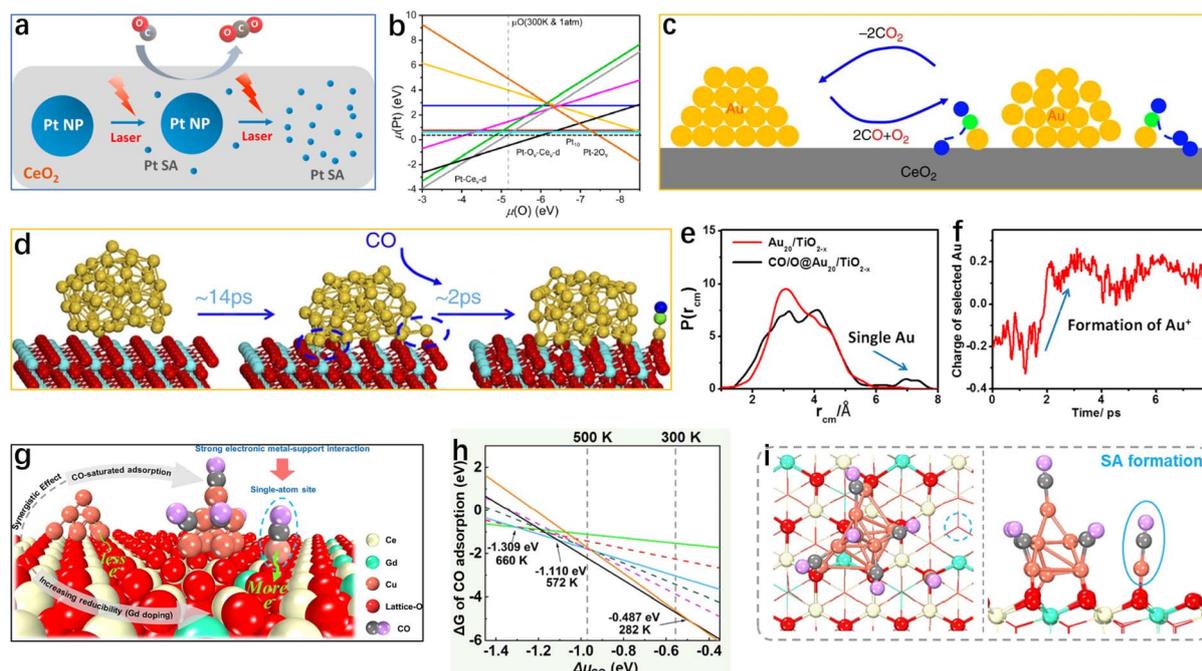

Fig. 5 (a) Achieve controlled conversion of Pt NPs to SAs on CeO$_2$ using a laser ablation strategy for enhanced CO oxidation efficiency. (b) The chemical potential of Pt at varying oxygen chemical potentials is calculated based on the configuration of the active center.[45] (c) Schematic illustration of the anticipated reaction mechanism for CO oxidation at the Au SAs. (d) Snapshots of dynamics structural evolution by the MD simulation for CeO$_2$-supported Au$_{50}$ cluster to SAs.[46] (e) Distribution function $P(r_{cm})$ of Au atoms relative to the center of mass of the Au-nanoparticle.[47] (f) The Mulliken charge of the isolated Au atom plotted against the simulation time after equilibration. (g) Schematic representation of the catalyst structures evolution of the Cu SAs formation process on Gd-doped CeO$_2$ surface.[82] (h) Gibbs free energy change calculated for multiple CO adsorptions on Cu$_{10}$/Gd$_{0.25}$Ce$_{0.75}$O$_2$ under CO oxidation conditions. (i) The top and side views of the most stable CO-saturated adsorption configuration on Cu$_{10}$/Gd$_{0.219}$Ce$_{0.781}$O$_2$.

the function $P(r_{cm})$ was employed to quantify the probability distribution of an Au atom positioned at a distance of r_{cm} from the center of mass of Au_{20} clusters. The peak observed around ~ 7 Å in $P(r_{cm})$ enables the clear identification of separated Au atoms, as shown in Fig. 5e. Upon detachment of the Au–CO unit from the cluster, the charge state of Au shifts from negative within the cluster to positive in the SAs (Fig. 5f). This transition suggests that, similar to CeO_2, the active species is best represented as an O_{ad}–Au^+–CO unit.[47]

Recently, Liu et al.[82] investigated the transformation of metal Cu clusters to SAs (Fig. 5g), focusing on how Gd-doping influences the electronic interactions between the metal and support. They explored the combined effect of Gd-doped CeO_2 and CO adsorption in the formation of single-atom sites. Through DFT calculations (Fig. 5h), they analyzed the Gibbs free energy changes associated with multiple CO molecules adsorbing onto Gd-doped CeO_2-supported Cu clusters under CO oxidation conditions. Their *ab initio* thermodynamic analysis revealed that the adsorption of a sixth CO molecule causes the Cu–CO species to detach from the cluster (Fig. 5i), leading to the formation of active Cu single-atom sites. These findings underscore the importance of dynamic active site formation under reaction conditions and their significant role in CeO_2 and TiO_2.

On the M–N–C catalysts, Li et al.[42] observed a direct conversion of noble metal clusters into SAs at temperatures above 900 °C in an inert atmosphere. As shown in Fig. 6a, high-resolution high-angle annular dark field scanning transmission electron microscopy confirmed the dynamic structural shift from metal clusters to SAs. Statistical data on particle diameters and quantities at various temperatures are displayed in Fig. 6b and c. The average diameter of Pd clusters gradually increased from room temperature up to 900 °C, in contrast, the number of Pd clusters steadily decreased (Fig. 6b), indicating a concurrent process of sintering and atomization during the transformation from metal clusters to SAs. At 1000 °C, a Pd cluster with an initial 6.5 nm diameter decreased to 4.0 nm at 136 s, further to 1.9 nm at 150 s, and completely disappeared by 162 s (Fig. 6c). Additionally, DFT calculations were used to simulate the conversion of clusters to SAs. As shown in Fig. 6d, a more thermodynamically stable Pd single atom formation at the N_4 defect from the Pd_{10} clusters decomposition requires overcoming a kinetic barrier of 1.47 eV, accompanied by a significant exothermicity of 3.96 eV. In a separate study, heating $(PtNi)_n$/Zn-ZIF from room temperature to 600–900 °C in an inert atmosphere resulted in notable changes in the elemental distribution of Ni, Pt, and Zn. They also proposed a novel conversion mechanism for multiphase metal catalysts, involving atomic displacement between SAs and nano-alloys clusters. This process consists of the release and enrichment of Zn atoms from the CN substrate into nano-alloy clusters, and the migration of Ni atoms from nano-alloy clusters into the CN substrate, while Pt atoms remain distributed on the nano-alloy clusters throughout the entire transformation.[48]
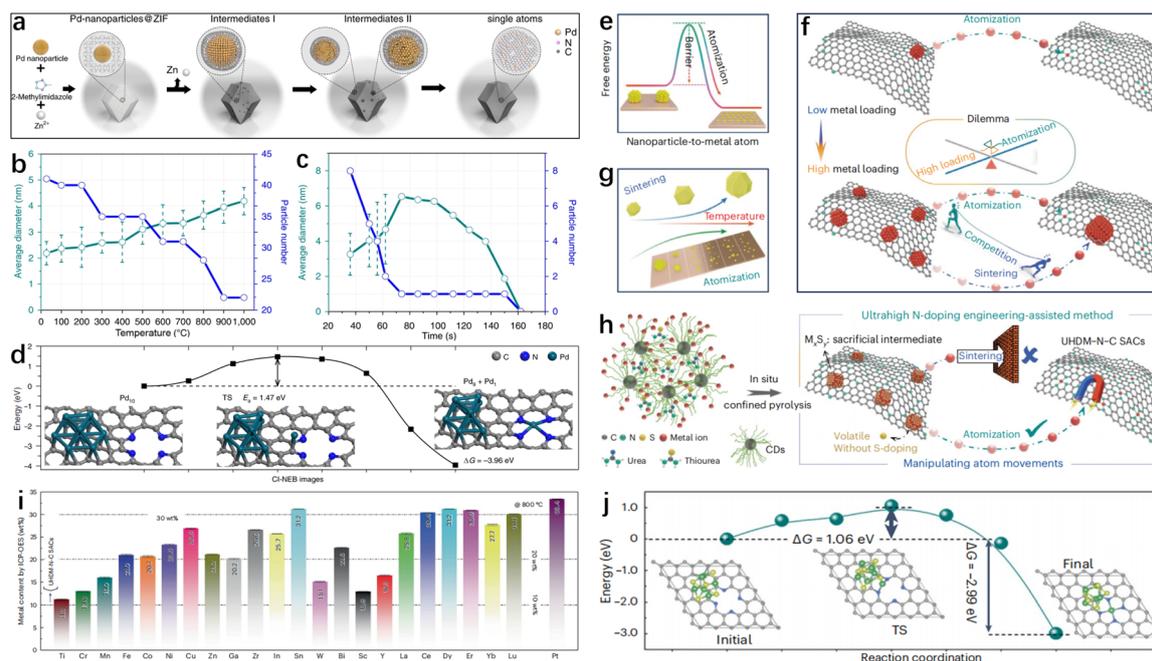

Fig. 6 (a) Schematic representation of the structural transformation from Pd NPs to SAs, depicted through high-resolution HAADF-STEM images. Average diameter and number of particles (b) *vs.* temperatures (c) *vs.* pyrolyzing time at 1000 °C. (d) The kinetic barriers, and the corresponding initial and final configurations of the Pd atom from the Pd_{10} cluster to the Pd–N_4 defect.[42] (e) Scheme of the energy barrier for the structural transformation of metal NPs to SAs. (f) The thermally driven atomization process transforming NPs to SAs is facilitated by adjacent N-dopants. (g) Schematic of the balance between achieving atomization and high loading while avoiding unwanted sintering during temperature-driven atomization. (h) The proposed strategy of high N-doping-assisted atomization enables the transformation of M_xS_y clusters into highly dispersed single metal atoms. (i) The ultrahigh metal loadings achieved for 23 different ultrahigh-density M–N–C SACs. (j) The kinetic barriers, and the corresponding initial and final configurations for the dynamic Ni atom dissociation from bulk NiS.[43]

The preparation of SAs by heat-driven direct transformation of metal clusters has been widely studied in above mentioned works. In theory, the structural transformation must overcome a kinetic barrier (Fig. 6e), thereby necessitating high temperatures to provide the requisite energy. Furthermore, methods for converting metal clusters to SAs are still challenged by low metal loading, primarily due to limited stabilization for mobile metal atoms. Introducing high metal content often leads to reaggregation from elevated surface free energy (Fig. 6f). High temperatures can intensify competitive atomization and sintering reactions, resulting in a tradeoff between achieving high metal atomic loading and mitigating sintering (Fig. 6g). Lu et al.[43] present a high N-doping-assisted atomization strategy that directly transforms M_xS_y clusters into ultra-high density (UHD) SACs. As illustrated in Fig. 6h, they developed N-doped carbon supports with substantial nitrogen content to selectively control the migration pathway of metal atoms, favoring atomization over sintering. This approach effectively bypasses the usual trade-off between high loading and aggregation, thereby enhancing M–N–C loading. Among the 23 UHDM–N–C SACs, 17 metals exhibit loadings exceeding 20%, with 6 metals (Sn, Ce, Er, Dy, Pt, and Lu) showing loadings greater than 30% (Fig. 6i). CI-NEB calculations reveal that releasing a Ni atom requires a kinetic barrier of 1.06 eV (Fig. 6j). Theoretical results suggest that increasing the temperature facilitates the transformation of M_xS_y clusters into metal SAs, which aligns with the experimental observation of the thermal-driven decomposition of NiS clusters during the preparation of UHDNi–N–C SACs.

Zhang et al.[83] utilized Co/Zn-ZIF as a precursor for pyrolysis, reporting the first observation of the evolution of Co SAs alongside the formation of a porous N-doped carbon support. Their study revealed that Co species underwent a dynamic cycle of agglomeration, dispersion, reagglomeration, and sublimation. In situ TEM and XAFS characterizations confirmed the stability of Co SAs on the porous CN_x carriers, which demonstrated an exceptional catalytic performance for the selective oxidation of ethylbenzene into acetophenone.

Notably, the above working preparation process requires additional energy to break strong metal–metal bonds and inhibit agglomeration to maintain atomic-level dispersion, which makes it difficult to control the purity and uniformity of SAs samples. Very recently, Wang et al.[84] demonstrated a novel, efficient, and simple strategy of electrochemically knocking-down Zn clusters into SAs (Fig. 7a): metal organic framework precursor derived from defects rich in Zn clusters carbon material as a starting point, through the controlled multi-cycle electrochemical lithiation/delithiation process, makes Zn clusters on carbon substrates to SAs. Using synchrotron radiation-based X-ray absorption near edge spectroscopy (XANES), they explore the coordination structure of Zn atoms to build a model that accurately represents real experimental conditions. The Zn K-edge XANES analysis depicted in Fig. 7b indicates that, compared with Zn SA–carbon, the position of the absorption edge for the Zn SA/cluster-carbon slightly shifts to large photon energy, revealing that the presence of a mixed oxidation state of Zn ranging between 0 and +2 originates from the Zn clusters and SAs. Subsequently, they used EXAFS spectra to
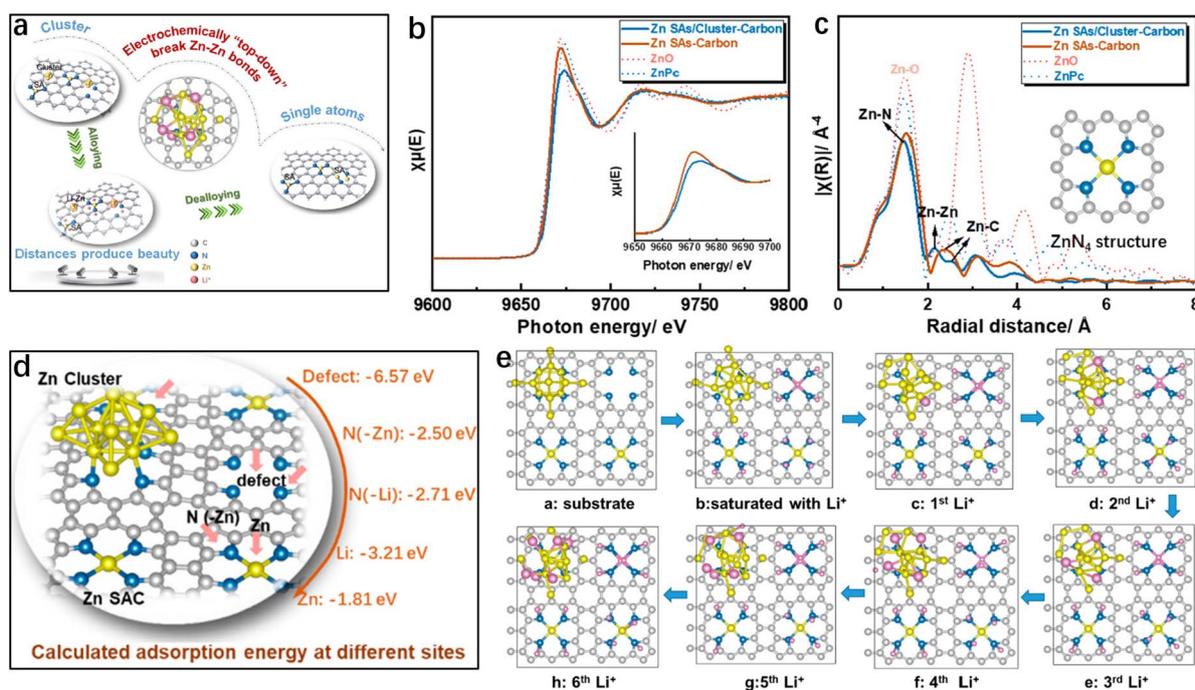

Fig. 7 (a) Schematic illustration of a novel, simple electrochemical knock-down approach for inducing structural evolution from Zn clusters into SAs.[84] (b) Zn K-edge XANES spectra and (c) FT-EXAFS spectra of Zn SA/cluster-carbon and Zn SA–carbon, along with ZnO and ZnPc standard samples. (d) The calculated adsorption energy of Li⁺ on all possible adsorption sites. (e) The conversion pathway of metal Zn clusters into individual SAs during the alloying/dealloying process.
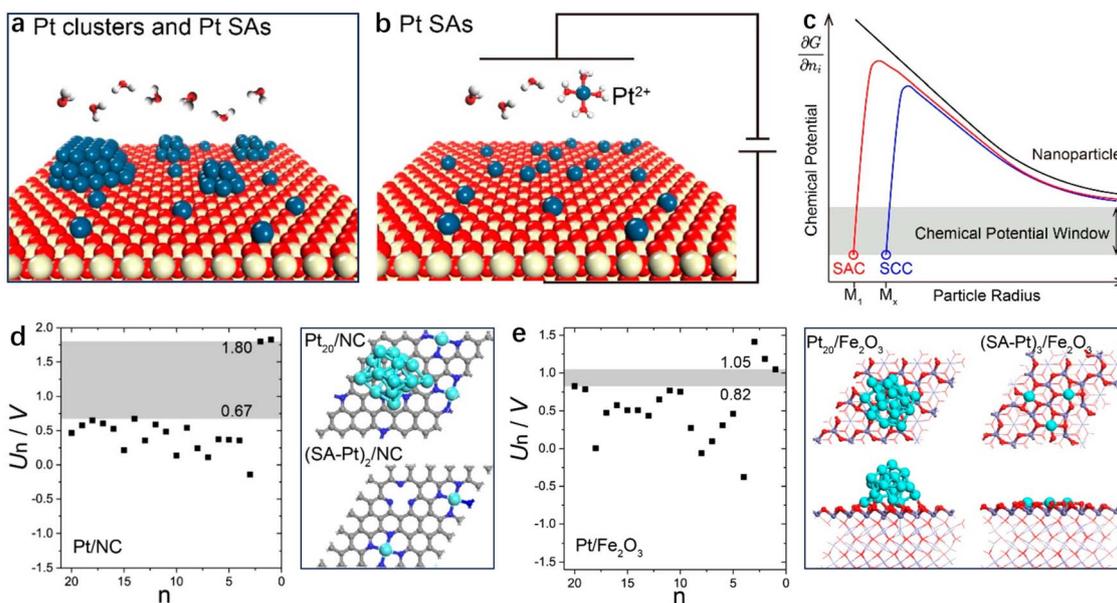
Fig. 8 Schematic illustrations depicting (a) pre-deposited Pt on the substrate in the form of clusters and SAs, (b) SAs remaining on the substrate following selective leaching within the electrochemical potential window, and (c) typical trends of chemical potentials ($\partial G/\partial n_i$) with particle size under three typical conditions. Threshold leaching potentials U_n for Pt_n ($n = 20-1$) support in (d) NC and (e) Fe_2O_3.[85]

quantitatively determine the coordination of the Zn atoms. As shown in Fig. 7c, apart from the primary Zn–N peak, the second most prominent peak in Zn SA/cluster-carbon is the Zn–Zn peak, which indicates the coexistence of Zn SAs and clusters.

To further validate the observed conversion of Zn clusters to SAs, they constructed a model incorporating defects, Zn–N$_4$ coordination, and Zn clusters for DFT calculations. Adsorption energies of Li$^+$ at different sites are described in Fig. 7d, Li$^+$ would preferentially adsorb on the defects and Zn–N$_4$ sites compared with that of Zn cluster sites, the active sites in the model are initially saturated with Li$^+$ to facilitate a more detailed analysis of the specific interactions between Li$^+$ and Zn clusters. As shown in Fig. 7e, the strong adsorption energy of Li$^+$ indicates that Li$^+$ can easily combine with Zn clusters, facilitating an alloying reaction. In addition, upon the interaction of the fifth Li$^+$ with Zn clusters, the Zn atom appears to escape significantly, indicating that the Zn–Zn bond can be destroyed after enough Zn–Li bonds are established. These liberated Zn atoms are efficiently captured by numerous Zn–N$_4$ defects, leading to the creation of new Zn monatomic sites. This significant finding marks the behavior of metal cluster dynamics, paving the way for creating innovative materials through the direct transformation of metal clusters into SAs.

An efficient strategy for producing high-purity and high-loading metal SAs involves starting with a well-defined substrate and predepositing metal atoms using conventional techniques, without the need for precise control. As illustrated in Fig. 8a–c, Liu *et al.*[85] discovered that under an applied voltage, there is a sufficiently wide electrochemical potential window in which all metal species, except for the tightly bound SAs, are oxidized and leached out. For this method to be effective, the substrate must exhibit a strong enough binding to the specific SAs, ensuring that the chemical potential of the metal in the SAs is lower than in the metal clusters. Provided this condition is met, their theoretical results suggest that the strategy can successfully produce high-loading and high-purity SAs, even when the substrate surface contains clusters of varying sizes.

The threshold potential (U_n) required for leaching each metal atom was subsequently calculated. As shown in Fig. 8d, at $U = 0.67$ V, all 18 Pt atoms forming the Pt clusters at single vacancies leach into the aqueous solution as Pt^{2+}, while two Pt SAs remain at double vacancies coordinated by four nitrogen atoms. Leaching of these two Pt SAs requires $U > 1.80$ V on NC. Similarly, Fig. 8e illustrates a chemical potential window of 0.23 V (between leaching potentials of 0.82 and 1.05 V) that facilitates the simple preparation of Pt/Fe$_2$O$_3$ SACs. The findings indicate that, apart from the strongly bound SAs, all forms of Pt undergo electrochemical leaching and dissolution from the NC and Fe$_2$O$_3$ surfaces into the electrolyte, providing an efficient strategy for preparing high-purity and high-loading Pt SACs without the need for precise control of Pt chemical potential. Additionally, the strategy's versatility is demonstrated by modeling the synthesis of Pd and Ni SACs anchored on NC and Fe$_2$O$_3$.

3   Summary and perspective

This review discusses how the dynamic structural evolution of metal SAs and clusters is highly dependent on reaction conditions such as applied potential, reactants, coordinative structures, thermal treatment, and metal particle size, all of which impact their transformations. Gaining insight into the mechanisms driving the evolution of singly dispersed metal atoms and clusters offers valuable information on the true active sites, as

well as on the processes by which the catalyst is activated and deactivated throughout the catalytic cycle.

Dynamic structural evolution of metal SAs and clusters presents a significant challenge in identifying the catalytically active species. *Ex situ* characterizations may fail to capture true active sites, as metal SAs can aggregate into clusters or reaction-induced clusters may convert into isolated atoms by the reaction's end. Therefore, *operando* characterizations under realistic working conditions are essential to prevent inaccurate or misleading conclusions.

Researchers have made significant efforts to identify the true active sites in catalysts, but there remains disagreement about the contributions of metal clusters and single atomic sites to catalyst activity. Recently, an effective approach has been to combine metal sites with distinct structures onto a catalyst substrate, where these varied sites work in coordination to facilitate the overall reaction process through a division-of-labor strategy. The site with the highest intrinsic activity functions as the primary reaction site, while another metal species serves as a dopant to modulate the electronic structure of the active site. The synergistic effect between the composite catalysts consisting of metal clusters and SAs can tune the electronic structure of the active site, thereby enhancing its inherent activity. By incorporating two sites optimized for different catalytic reactions, bifunctional catalysis can be exploited to improve the efficiency of multi-step catalytic reactions.[86–114] This underscores the importance of synergistic catalysis between metal clusters and SAs in optimizing catalytic efficiency. However, to date, no studies have addressed the dynamic structural evolution of this synergistic effect. A comprehensive theory to explain or predict the behavior of metal catalysts with varying particle sizes under different reaction conditions remains unexplored, which will be the focus of future research.

However, there are inherent limitations for real-time simulation of the catalytic reactions under operative conditions: (i) the elementary steps may occur at different locations of the catalyst, and accurately identifying the structure and dynamic evolution of the active site of the electrocatalyst during the catalytic reaction is a necessary condition for exploring the sources of the activity of the catalyst and understanding the mechanism of catalytic reaction. However, monitoring the real-time evolution of catalyst structural complexity is a significant challenge. (ii) The dynamic change of the structure can affect the kinetics of catalytic reactions, leading to different pathways and products. Therefore, developing a theoretical approach that integrates structural dynamics with reaction kinetics is crucial for simulating catalytic reactions. (iii) Establishing a reliable structure–activity relationship from the onset of the reaction to catalyst deactivation presents a significant challenge. In principle, this relationship is determined by comparing two different and clearly defined structures under the same reaction conditions. However, this task becomes extremely difficult due to the dynamical evolution of the catalyst structure and the complexity of its changes with the reaction conditions.

In summary, this review highlights the dynamic evolution of metal SAs and clusters in various catalytic reactions, showcasing the complexity and diversity of active site structures in catalysis. It emphasizes the significance of dynamic structural changes of metal species under operating conditions and identifies the challenges current theoretical methods face in simulating these changes. To gain a comprehensive understanding of reaction mechanisms and design efficient catalysts with optimized active site structures, it is crucial to focus on the dynamic evolution of the active center. This requires integrating catalyst structural dynamics with reaction kinetics through the development of novel theoretical frameworks and advanced *in situ*/*operando* characterization techniques.

Data availability

No primary research results, software, or code have been included and no new data were generated or analyzed as part of this review.

Author contributions

All of the authors contributed to the manuscript preparation. S. W., J. M. and D. M. conceived the outline of the manuscript. S. W. wrote the original draft of the manuscript. C. L., W. H., Y. Z., J. C., X. Z., L. W., X. N. and Q. Z. discussed and helped revise the manuscript.

Conflicts of interest

The authors declare no competing financial interest.

Acknowledgements

References

1 A. T. Bell, The Impact of Nanoscience on Heterogeneous Catalysis, *Science*, 2003, **299**, 1688–1691.

2 F. Tao and P. A. Crozier, Atomic-Scale Observations of Catalyst Structures under Reaction Conditions and during Catalysis, *Chem. Rev.*, 2016, **116**, 3487–3539.

3 B. Zhu, J. Meng, W. Yuan, X. Zhang, H. Yang, Y. Wang and Y. Gao, Reshaping of Metal Nanoparticles Under Reaction Conditions, *Angew. Chem., Int. Ed.*, 2020, **59**, 2171–2180.

4 G. Wan, G. Zhang, J. Z. Chen, M. F. Toney, J. T. Miller and C. J. Tassone, Reaction-Mediated Transformation of Working Catalysts, *ACS Catal.*, 2022, **12**, 8007–8018.

5 J. Jones, H. Xiong, A. T. DeLaRiva, E. J. Peterson, H. Pham, S. R. Challa, G. Qi, S. Oh, M. H. Wiebenga, X. I. Pereira

Hernández, Y. Wang and A. K. Datye, Thermally stable single-atom platinum-on-ceria catalysts *via* atom trapping, *Science*, 2016, **353**, 150–154.

6 R. Lang, W. Xi, J.-C. Liu, Y.-T. Cui, T. Li, A. F. Lee, F. Chen, Y. Chen, L. Li, L. Li, J. Lin, S. Miao, X. Liu, A.-Q. Wang, X. Wang, J. Luo, B. Qiao, J. Li and T. Zhang, Non defect-stabilized thermally stable single-atom catalyst, *Nat. Commun.*, 2019, **10**, 234.

7 Z. Li, S. Ji, Y. Liu, X. Cao, S. Tian, Y. Chen, Z. Niu and Y. Li, Well-Defined Materials for Heterogeneous Catalysis: From Nanoparticles to Isolated Single-Atom Sites, *Chem. Rev.*, 2020, **120**, 623–682.

8 L. Liu and A. Corma, Metal Catalysts for Heterogeneous Catalysis: From Single Atoms to Nanoclusters and Nanoparticles, *Chem. Rev.*, 2018, **118**, 4981–5079.

9 M. A. Newton, Dynamic adsorbate/reaction induced structural change of supported metal nanoparticles: heterogeneous catalysis and beyond, *Chem. Soc. Rev.*, 2008, **37**, 2644–2657.

10 X.-F. Yang, A. Wang, B. Qiao, J. Li, J. Liu and T. Zhang, Single-Atom Catalysts: A New Frontier in Heterogeneous Catalysis, *Acc. Chem. Res.*, 2013, **46**, 1740–1748.

11 A. Wang, J. Li and T. Zhang, Heterogeneous single-atom catalysis, *Nat. Rev. Chem*, 2018, **2**, 65–81.

12 W. Zhang and W. Zheng, Single Atom Excels as the Smallest Functional Material, *Adv. Funct. Mater.*, 2016, **26**, 2988–2993.

13 N. Cheng, L. Zhang, K. Doyle-Davis and X. Sun, Single-Atom Catalysts: From Design to Application, *Electrochem. Energy Rev.*, 2019, **2**, 539–573.

14 J. Zhang, W. Cai, F. X. Hu, H. Yang and B. Liu, Recent advances in single atom catalysts for the electrochemical carbon dioxide reduction reaction, *Chem. Sci.*, 2021, **12**, 6800–6819.

15 H.-Y. Zhuo, X. Zhang, J.-X. Liang, Q. Yu, H. Xiao and J. Li, Theoretical Understandings of Graphene-based Metal Single-Atom Catalysts: Stability and Catalytic Performance, *Chem. Rev.*, 2020, **120**, 12315–12341.

16 S. Ding, M. J. Hülsey, J. Pérez-Ramírez and N. Yan, Transforming energy with single-atom catalysts, *Joule*, 2019, **3**, 2897–2929.

17 W. Guo, X. Tan, J. Bi, L. Xu, D. Yang, C. Chen, Q. Zhu, J. Ma, A. Tayal, J. Ma, Y. Huang, X. Sun, S. Liu and B. Han, Atomic Indium Catalysts for Switching CO₂ Electroreduction Products from Formate to CO, *J. Am. Chem. Soc.*, 2021, **143**, 6877–6885.

18 C. Tang, L. Chen, H. Li, L. Li, Y. Jiao, Y. Zheng, H. Xu, K. Davey and S.-Z. Qiao, Tailoring Acidic Oxygen Reduction Selectivity on Single-Atom Catalysts *via* Modification of First and Second Coordination Spheres, *J. Am. Chem. Soc.*, 2021, **143**, 7819–7827.

19 K. Liu, J. Fu, Y. Lin, T. Luo, G. Ni, H. Li, Z. Lin and M. Liu, Insights into the activity of single-atom Fe-N-C catalysts for oxygen reduction reaction, *Nat. Commun.*, 2022, **13**, 2075.

20 Y. Yang, J. Fu, Y. Ouyang, T. Tang, Y. Zhang, L.-R. Zheng, Q.-H. Zhang, X.-Z. Liu, J. Wang and J.-S. Hu, In-situ constructed Cu/CuNC interfaces for low-overpotential

21 reduction of CO₂ to ethanol, *Natl. Sci. Rev.*, 2023, **10**, nwac248.

21 Y. Guo, S. Mei, K. Yuan, D.-J. Wang, H.-C. Liu, C.-H. Yan and Y.-W. Zhang, Low-Temperature CO₂ Methanation over CeO₂-Supported Ru Single Atoms, Nanoclusters, and Nanoparticles Competitively Tuned by Strong Metal–Support Interactions and H-Spillover Effect, *ACS Catal.*, 2018, **8**, 6203–6215.

22 H. Xiong, S. Lin, J. Goetze, P. Pletcher, H. Guo, L. Kovarik, K. Artyushkova, B. M. Weckhuysen and A. K. Datye, Thermally Stable and Regenerable Platinum–Tin Clusters for Propane Dehydrogenation Prepared by Atom Trapping on Ceria, *Angew. Chem., Int. Ed.*, 2017, **129**, 9114–9119.

23 Q. Li, Y. Zhang, L. Shi, M. Wu, Y. Ouyang and J. Wang, Dynamic structure change of Cu nanoparticles on carbon supports for CO electro-reduction toward multicarbon products, *InfoMat*, 2021, **3**, 1285–1294.

24 C. Dong, Z. Gao, Y. Li, M. Peng, M. Wang, Y. Xu, C. Li, M. Xu, Y. Deng, X. Qin, F. Huang, X. Wei, Y.-G. Wang, H. Liu, W. Zhou and D. Ma, Fully exposed palladium cluster catalysts enable hydrogen production from nitrogen heterocycles, *Nat. Catal.*, 2022, **5**, 485–493.

25 L. Liu and A. Corma, Evolution of isolated atoms and clusters in catalysis, *Trends Chem.*, 2020, **2**, 383–400.

26 Y. Gao and B. Zhu, Simulating Structural Dynamics of Metal Catalysts under Operative Conditions, *J. Phys. Chem. Lett.*, 2024, **15**, 8351–8359.

27 H. Yang, P. Duan, Z. Zhuang, Y. Luo, J. Shen, Y. Xiong, X. Liu and D. Wang, Understanding the Dynamic Evolution of Active Sites among Single Atoms, Clusters, and Nanoparticles, *Adv. Mater.*, 2025, **37**, 2415265.

28 X. Zhao, Z. H. Levell, S. Yu and Y. Liu, Atomistic Understanding of Two-dimensional Electrocatalysts from First Principles, *Chem. Rev.*, 2022, **122**, 10675–10709.

29 H. Hu, J. Wang, P. Tao, C. Song, W. Shang, T. Deng and J. Wu, Stability of single-atom catalysts for electrocatalysis, *J. Mater. Chem. A*, 2022, **10**, 5835–5849.

30 Y. Yang, L. Lai, L. Wei and Y. Chen, Degradation: a critical challenge for M–N–C electrocatalysts, *J. Energy Chem.*, 2021, **63**, 667–674.

31 B.-C. Ye, W.-H. Li, X. Zhang, J. Chen, Y. Gao, D. Wang and H. Pan, Advancing Heterogeneous Organic Synthesis With Coordination Chemistry-Empowered Single-Atom Catalysts, *Adv. Mater.*, 2024, **36**, 2402747.

32 Z. Lang, X. Wang, S. Jabeen, Y. Cheng, N. Liu, Z. Liu, T. Gan, Z. Zhuang, H. Li and D. Wang, Destabilization of Single-Atom Catalysts: Characterization, Mechanisms, and Regeneration Strategies, *Adv. Mater.*, 2025, **37**, 2418942.

33 T. Gan and D. Wang, Atomically dispersed materials: Ideal catalysts in atomic era, *Nano Res.*, 2024, **17**, 18–38.

34 P. Liu, Y. Liu, K. Wang, S. Shi, M. Jin, J. Liu, T. Qin, Q. Liu, X. Liu and J. He, Revealing the role of electrode potential micro-environments in single Mn atoms for carbon dioxide and oxygen electrolysis, *Nano Res.*, 2024, **17**, 7957–7966.

35 C. E. Creissen and M. Fontecave, Keeping sight of copper in single-atom catalysts for electrochemical carbon dioxide reduction, *Nat. Commun.*, 2022, **13**, 2280.

36 L. Zhang, J. Yang, X. Yang, A. Wang and T. Zhang, Structural evolution of single-atom catalysts, *Chem Catal.*, 2023, **3**, 100560.

37 Y. Nian, X. Huang, M. Liu, J. Zhang and Y. Han, Insight into the Dynamic Evolution of Supported Metal Catalysts by In Situ/Operando Techniques and Theoretical Simulations, *ACS Catal.*, 2023, **13**, 11164–11171.

38 J. Yang, H. Qi, A. Li, X. Liu, X. Yang, S. Zhang, Q. Zhao, Q. Jiang, Y. Su, L. Zhang, J.-F. Li, Z.-Q. Tian, W. Liu, A. Wang and T. Zhang, Potential-Driven Restructuring of Cu Single Atoms to Nanoparticles for Boosting the Electrochemical Reduction of Nitrate to Ammonia, *J. Am. Chem. Soc.*, 2022, **144**, 12062–12071.

39 Y. Qin, W. Zhao, C. Xia, L.-J. Yu, F. Song, J. Zhang, T. Wu, R. Cao, S. Ding, B. Y. Xia and Y. Su, CO Intermediate-Assisted Dynamic Cu Sintering During Electrocatalytic CO_2 Reduction on Cu–N–C Catalysts, *Angew. Chem., Int. Ed.*, 2024, **63**, e202404763.

40 X. Bai, X. Zhao, Y. Zhang, C. Ling, Y. Zhou, J. Wang and Y. Liu, Dynamic Stability of Copper Single-Atom Catalysts under Working Conditions, *J. Am. Chem. Soc.*, 2022, **144**, 17140–17148.

41 Y. Zang, S. Wang, J. Sang, P. Wei, X. Zhang, Q. Wang and G. Wang, Illustration of the Intrinsic Mechanism of Reconstructed Cu Clusters for Enhanced CO_2 Electroreduction to Ethanol Production with Industrial Current Density, *Nano Lett.*, 2024, **24**, 7261–7268.

42 S. Wei, A. Li, J.-C. Liu, Z. Li, W. Chen, Y. Gong, Q. Zhang, W.-C. Cheong, Y. Wang, L. Zheng, H. Xiao, C. Chen, D. Wang, Q. Peng, L. Gu, X. Han, J. Li and Y. Li, Direct observation of noble metal nanoparticles transforming to thermally stable single atoms, *Nat. Nanotechnol.*, 2018, **13**, 856–861.

43 J. Chang, W. Jing, X. Yong, A. Cao, J. Yu, H. Wu, C. Wan, S. Wang, G. I. N. Waterhouse, B. Yang, Z. Tang, X. Duan and S. Lu, Synthesis of ultrahigh-metal-density single-atom catalysts via metal sulfide-mediated atomic trapping, *Nat. Synth.*, 2024, **3**, 1427–1438.

44 C. Dessal, T. Len, F. Morfin, J.-L. Rousset, M. Aouine, P. Afanasiev and L. Piccolo, Dynamics of Single Pt Atoms on Alumina during CO Oxidation Monitored by Operando X-ray and Infrared Spectroscopies, *ACS Catal.*, 2019, **9**, 5752–5759.

45 N. Fu, X. Liang, X. Wang, T. Gan, C. Ye, Z. Li, J.-C. Liu and Y. Li, Controllable Conversion of Platinum Nanoparticles to Single Atoms in Pt/CeO2 by Laser Ablation for Efficient CO Oxidation, *J. Am. Chem. Soc.*, 2023, **145**, 9540–9547.

46 Y.-G. Wang, D. Mei, V.-A. Glezakou, J. Li and R. Rousseau, Dynamic formation of single-atom catalytic active sites on ceria-supported gold nanoparticles, *Nat. Commun.*, 2015, **6**, 6511.

47 Y.-G. Wang, D. C. Cantu, M.-S. Lee, J. Li, V.-A. Glezakou and R. Rousseau, CO Oxidation on Au/TiO2: Condition-Dependent Active Sites and Mechanistic Pathways, *J. Am. Chem. Soc.*, 2016, **138**, 10467–10476.

48 X. Wang, N. Fu, J.-C. Liu, K. Yu, Z. Li, Z. Xu, X. Liang, P. Zhu, C. Ye, A. Zhou, A. Li, L. Zheng, L.-M. Liu, C. Chen, D. Wang, Q. Peng and Y. Li, Atomic Replacement of PtNi Nanoalloys within Zn-ZIF-8 for the Fabrication of a Multisite CO_2 Reduction Electrocatalyst, *J. Am. Chem. Soc.*, 2022, **144**, 23223–23229.

49 H. Zhao, R. Yu, S. Ma, K. Xu, Y. Chen, K. Jiang, Y. Fang, C. Zhu, X. Liu, Y. Tang, L. Wu, Y. Wu, Q. Jiang, P. He, Z. Liu and L. Tan, The role of Cu_1–O_3 species in single-atom Cu/ZrO2 catalyst for CO_2 hydrogenation, *Nat. Catal.*, 2022, **5**, 818–831.

50 H. Wan, L. Qian, N. Gong, H. Hou, X. Dou, L. Zheng, L. Zhang and L. Liu, Size-Dependent Structures and Catalytic Properties of Supported Bimetallic PtSn Catalysts for Propane Dehydrogenation Reaction, *ACS Catal.*, 2023, **13**, 7383–7394.

51 G. S. Parkinson, Z. Novotny, G. Argentero, M. Schmid, J. Pavelec, R. Kosak, P. Blaha and U. Diebold, Carbon monoxide-induced adatom sintering in a Pd–Fe3O4 model catalyst, *Nat. Mater.*, 2013, **12**, 724–728.

52 M. Moliner, J. E. Gabay, C. E. Kliewer, R. T. Carr, J. Guzman, G. L. Casty, P. Serna and A. Corma, Reversible Transformation of Pt Nanoparticles into Single Atoms inside High-Silica Chabazite Zeolite, *J. Am. Chem. Soc.*, 2016, **138**, 15743–15750.

53 Z. Zhang, J. Tian, Y. Lu, S. Yang, D. Jiang, W. Huang, Y. Li, J. Hong, A. S. Hoffman, S. R. Bare, M. H. Engelhard, A. K. Datye and Y. Wang, Memory-dictated dynamics of single-atom Pt on CeO2 for CO oxidation, *Nat. Commun.*, 2023, **14**, 2664.

54 V. Giulimondi, S. K. Kaiser, M. Agrachev, F. Krumeich, A. H. Clark, S. Mitchell, G. Jeschke and J. Pérez-Ramírez, Redispersion strategy for high-loading carbon-supported metal catalysts with controlled nuclearity, *J. Mater. Chem. A*, 2022, **10**, 5953–5961.

55 Z. Pu, Z. Yin, X. Ma, J. Zhao and J. Zeng, In-situ adaptive evolution of rhodium oxide clusters into single atoms via mobile rhodium-adsorbate intermediates, *Chin. J. Catal.*, 2023, **48**, 247–257.

56 M. A. Albrahim, A. Shrotri, R. R. Unocic, A. S. Hoffman, S. R. Bare and A. M. Karim, Size-Dependent Dispersion of Rhodium Clusters into Isolated Single Atoms at Low Temperature and the Consequences for CO Oxidation Activity, *Angew. Chem., Int. Ed.*, 2023, **62**, e202308002.

57 J. Yang, W. Liu, M. Xu, X. Liu, H. Qi, L. Zhang, X. Yang, S. Niu, D. Zhou, Y. Liu, Y. Su, J.-F. Li, Z.-Q. Tian, W. Zhou, A. Wang and T. Zhang, Dynamic Behavior of Single-Atom Catalysts in Electrocatalysis: Identification of Cu-N3 as an Active Site for the Oxygen Reduction Reaction, *J. Am. Chem. Soc.*, 2021, **143**, 14530–14539.

58 L. Cao, Q. Luo, W. Liu, Y. Lin, X. Liu, Y. Cao, W. Zhang, Y. Wu, J. Yang, T. Yao and S. Wei, Identification of single-atom active sites in carbon-based cobalt catalysts during electrocatalytic hydrogen evolution, *Nat. Catal.*, 2019, **2**, 134–141.

59 H. Su, W. Zhou, H. Zhang, W. Zhou, X. Zhao, Y. Li, M. Liu, W. Cheng and Q. Liu, Dynamic Evolution of Solid–Liquid Electrochemical Interfaces over Single-Atom Active Sites, *J. Am. Chem. Soc.*, 2020, **142**, 12306–12313.

60 X. Li, C.-S. Cao, S.-F. Hung, Y.-R. Lu, W. Cai, A. I. Rykov, S. Miao, S. Xi, H. Yang, Z. Hu, J. Wang, J. Zhao, E. E. Alp, W. Xu, T.-S. Chan, H. Chen, Q. Xiong, H. Xiao, Y. Huang, J. Li, T. Zhang and B. Liu, Identification of the Electronic and Structural Dynamics of Catalytic Centers in Single-Fe-Atom Material, Chem, 2020, 6, 3440–3454.

61 X. Wang, K. Maeda, X. Chen, K. Takanabe, K. Domen, Y. Hou, X. Fu and M. Antonietti, Polymer Semiconductors for Artificial Photosynthesis: Hydrogen Evolution by Mesoporous Graphitic Carbon Nitride with Visible Light, J. Am. Chem. Soc., 2009, 131, 1680–1681.

62 X. Wang, X. Chen, A. Thomas, X. Fu and M. Antonietti, Metal-Containing Carbon Nitride Compounds: A New Functional Organic–Metal Hybrid Material, Adv. Mater., 2009, 21, 1609–1612.

63 Y. Wang, X. Wang and M. Antonietti, Polymeric Graphitic Carbon Nitride as a Heterogeneous Organocatalyst: From Photochemistry to Multipurpose Catalysis to Sustainable Chemistry, Angew. Chem., Int. Ed., 2012, 51, 68–89.

64 X. Wang, K. Maeda, A. Thomas, K. Takanabe, G. Xin, J. M. Carlsson, K. Domen and M. Antonietti, A metal-free polymeric photocatalyst for hydrogen production from water under visible light, Nat. Mater., 2009, 8, 76–80.

65 J. Zhang, X. Chen, K. Takanabe, K. Maeda, K. Domen, J. D. Epping, X. Fu, M. Antonietti and X. Wang, Synthesis of a Carbon Nitride Structure for Visible-Light Catalysis by Copolymerization, Angew. Chem., Int. Ed., 2009, 2, 451–454.

66 X. Chen, J. Zhang, X. Fu, M. Antonietti and X. Wang, Fe-g-C3N4-Catalyzed Oxidation of Benzene to Phenol Using Hydrogen Peroxide and Visible Light, J. Am. Chem. Soc., 2009, 131, 11658–11659.

67 S. Wang, L. Shi, X. Bai, Q. Li, C. Ling and J. Wang, Highly Efficient Photo-/Electrocatalytic Reduction of Nitrogen into Ammonia by Dual-Metal Sites, ACS Cent. Sci., 2020, 6, 1762–1771.

68 S. Wang, J. Li, Q. Li, X. Bai and J. Wang, Metal single-atom coordinated graphitic carbon nitride as an efficient catalyst for CO oxidation, Nanoscale, 2020, 12, 364–371.

69 Y. Zheng, Y. Jiao, Y. Zhu, Q. Cai, A. Vasileff, L. H. Li, Y. Han, Y. Chen and S.-Z. Qiao, Molecule-Level g-C3N4 Coordinated Transition Metals as a New Class of Electrocatalysts for Oxygen Electrode Reactions, J. Am. Chem. Soc., 2017, 139, 3336–3339.

70 W. Niu, K. Marcus, L. Zhou, Z. Li, L. Shi, K. Liang and Y. Yang, Enhancing Electron Transfer and Electrocatalytic Activity on Crystalline Carbon-Conjugated g-C3N4, ACS Catal., 2018, 8, 1926–1931.

71 Y. Wu, C. Li, W. Liu, H. Li, Y. Gong, L. Niu, X. Liu, C. Sun and S. Xu, Unexpected monoatomic catalytic-host synergetic OER/ORR by graphitic carbon nitride: density functional theory, Nanoscale, 2019, 11, 5064–5071.

72 Y. Jiao, Y. Zheng, P. Chen, M. Jaroniec and S.-Z. Qiao, Molecular Scaffolding Strategy with Synergistic Active Centers To Facilitate Electrocatalytic CO2 Reduction to Hydrocarbon/Alcohol, J. Am. Chem. Soc., 2017, 139, 18093–18100.

73 X. Liu, Y. Jiao, Y. Zheng, M. Jaroniec and S.-Z. Qiao, Building Up a Picture of the Electrocatalytic Nitrogen Reduction Activity of Transition Metal Single-Atom Catalysts, J. Am. Chem. Soc., 2019, 141, 9664–9672.

74 L. Zhang, X. Yang, Q. Yuan, Z. Wei, J. Ding, T. Chu, C. Rong, Q. Zhang, Z. Ye, F.-Z. Xuan, Y. Zhai, B. Zhang and X. Yang, Elucidating the structure-stability relationship of Cu single-atom catalysts using operando surface-enhanced infrared absorption spectroscopy, Nat. Commun., 2023, 14, 8311.

75 J. Zhang, Y. Wang and Y. Li, Not One, Not Two, But at Least Three: Activity Origin of Copper Single-Atom Catalysts toward CO2/CO Electroreduction to C2+ Products, J. Am. Chem. Soc., 2024, 146, 14954–14958.

76 X. Bai, Q. Li, L. Shi, X. Niu, C. Ling and J. Wang, Hybrid Cu0 and Cu+ as Atomic Interfaces Promote High-Selectivity Conversion of CO2 to C2H5OH at Low Potential, Small, 2020, 16, 1901981.

77 Y. Yang, S. Louisia, S. Yu, J. Jin, I. Roh, C. Chen, M. V. Fonseca Guzman, J. Feijóo, P.-C. Chen, H. Wang, C. J. Pollock, X. Huang, Y.-T. Shao, C. Wang, D. A. Muller, H. D. Abruña and P. Yang, Operando studies reveal active Cu nanograins for CO2 electroreduction, Nature, 2023, 614, 262–269.

78 L. Xu, K. G. Papanikolaou, B. A. J. Lechner, L. Je, G. A. Somorjai, M. Salmeron and M. Mavrikakis, Formation of active sites on transition metals through reaction-driven migration of surface atoms, Science, 2023, 380, 70–76.

79 P. Hou, Q. Yu, F. Luo and J.-C. Liu, Reactant-Induced Dynamic Active Sites on Cu Catalysts during the Water–Gas Shift Reaction, ACS Catal., 2025, 15, 352–360.

80 X. Wei, Y. Liu, X. Zhu, S. Bo, L. Xiao, C. Chen, T. T. T. Nga, Y. He, M. Qiu, C. Xie, D. Wang, Q. Liu, F. Dong, C.-L. Dong, X.-Z. Fu and S. Wang, Dynamic Reconstitution Between Copper Single Atoms and Clusters for Electrocatalytic Urea Synthesis, Adv. Mater., 2023, 35, 2300020.

81 B. Qiao, A. Wang, X. Yang, L. F. Allard, Z. Jiang, Y. Cui, J. Liu, J. Li and T. Zhang, Single-atom catalysis of CO oxidation using Pt1/FeOx, Nat. Chem., 2011, 3, 634–641.

82 D. Liu, H. Zhu, X. Gong, S. Yuan, H. Ma, P. He, Y. Fan, W. Zhao, H. Ren and W. Guo, Understanding and controlling the formation of single-atom site from supported Cu10 cluster by tuning CeO2 reducibility: Theoretical insight into the Gd-doping effect on electronic metal-support interaction, J. Colloid Interface Sci., 2024, 661, 720–729.

83 L. Zhang, Y. Li, L. Zhang, K. Wang, Y. Li, L. Wang, X. Zhang, F. Yang and Z. Zheng, Direct Visualization of the Evolution of a Single-Atomic Cobalt Catalyst from Melting Nanoparticles with Carbon Dissolution, Adv. Sci., 2022, 9, 2200592.

84 J. Sun, J. Yang, T. Wang, S. L. Zhang, H. Yuan, W. Zang, Y. Liu, X. Liu, W. Wang, S. Xi, C. H. Kirk, H. Wang, J. Wang, X. Wang, U. Bhat, Z. Liu, S. Wang, Y.-W. Zhang and J. Wang, Electrochemical Knocking-Down of Zn Metal Clusters into Single Atoms, Nano Lett., 2024, 24, 5206–5213.

85 J.-C. Liu, H. Xiao and J. Li, Constructing High-Loading Single-Atom/Cluster Catalysts *via* an Electrochemical Potential Window Strategy, *J. Am. Chem. Soc.*, 2020, **142**, 3375–3383.

86 C. Wang, X. Wang, H. Ren, Y. Zhang, X. Zhou, J. Wang, Q. Guan, Y. Liu and W. Li, Combining Fe nanoparticles and pyrrole-type Fe-N_4 sites on less-oxygenated carbon supports for electrochemical CO_2 reduction, *Nat. Commun.*, 2023, **14**, 5108.

87 Y. Yu, X. a. Dong, P. Chen, Q. Geng, H. Wang, J. Li, Y. Zhou and F. Dong, Synergistic Effect of Cu Single Atoms and Au–Cu Alloy Nanoparticles on TiO_2 for Efficient CO_2 Photoreduction, *ACS Nano*, 2021, **15**, 14453–14464.

88 L. Zeng, Z. Zhao, Q. Huang, C. Zhou, W. Chen, K. Wang, M. Li, F. Lin, H. Luo, Y. Gu, L. Li, S. Zhang, F. Lv, G. Lu, M. Luo and S. Guo, Single-Atom Cr–N_4 Sites with High Oxophilicity Interfaced with Pt Atomic Clusters for Practical Alkaline Hydrogen Evolution Catalysis, *J. Am. Chem. Soc.*, 2023, **145**, 21432–21441.

89 Z. Ma, S. Liu, N. Tang, T. Song, K. Motokura, Z. Shen and Y. Yang, Coexistence of Fe Nanoclusters Boosting Fe Single Atoms to Generate Singlet Oxygen for Efficient Aerobic Oxidation of Primary Amines to Imines, *ACS Catal.*, 2022, **12**, 5595–5604.

90 X. Li, J. Liu, J. Wu, L. Zhang, D. Cao and D. Cheng, Constructing a Highly Active Pd Atomically Dispersed Catalyst for Cinnamaldehyde Hydrogenation: Synergistic Catalysis between Pd–N_3 Single Atoms and Fully Exposed Pd Clusters, *ACS Catal.*, 2024, **14**, 2369–2379.

91 R. Chen, S. Chen, L. Wang and D. Wang, Nanoscale Metal Particle Modified Single-Atom Catalyst: Synthesis, Characterization, and Application, *Adv. Mater.*, 2024, **36**, 2304713.

92 F. Mo, Q. Zhou, W. Xue, W. Liu, S. Xu, Z. Hou, J. Wang and Q. Wang, The Optimized Catalytic Performance of Single-Atom Catalysts by Incorporating Atomic Clusters or Nanoparticles: In-Depth Understanding on Their Synergisms, *Adv. Energy Mater.*, 2023, **13**, 2301711.

93 X. Yang, Y. Wang, X. Wang, B. Mei, E. Luo, Y. Li, Q. Meng, Z. Jin, Z. Jiang, C. Liu, J. Ge and W. Xing, CO-Tolerant PEMFC Anodes Enabled by Synergistic Catalysis between Iridium Single-Atom Sites and Nanoparticles, *Angew. Chem., Int. Ed.*, 2021, **60**, 26177–26183.

94 S. Yin, H. Yi, M. Liu, J. Yang, S. Yang, B.-W. Zhang, L. Chen, X. Cheng, H. Huang, R. Huang, Y. Jiang, H. Liao and S. Sun, An *in situ* exploration of how Fe/N/C oxygen reduction catalysts evolve during synthesis under pyrolytic conditions, *Nat. Commun.*, 2024, **15**, 6229.

95 C. Zhou, J. Shi, Z. Dong, L. Zeng, Y. Chen, Y. Han, L. Li, W. Zhang, Q. Zhang, L. Gu, F. Lv, M. Luo and S. Guo, Oxophilic gallium single atoms bridged ruthenium clusters for practical anion-exchange membrane electrolyzer, *Nat. Commun.*, 2024, **15**, 6741.

96 F. Mo, C. Song, Q. Zhou, W. Xue, S. Ouyang, Q. Wang, Z. Hou, S. Wang and J. Wang, The optimized Fenton-like activity of Fe single-atom sites by Fe atomic clusters–

97 Z. Li, M. Xu, J. Wang, Y. Zhang, W. Liu, X. Gu, Z.-K. Han, W. Ye and G. Li, Boosting Up Electrosynthesis of Urea with Nitrate and Carbon Dioxide *via* Synergistic Effect of Metallic Iron Cluster and Single-Atom, *Small*, 2024, **20**, 2400036.

98 Y. Wu, X. Tang, K. Yuan and Y. Chen, Single-atom sites combined with metal nano-aggregates for efficient electrocatalysis, *Energy Environ. Sci.*, 2023, **16**, 5663–5687.

99 J. Feng, L. Zhang, S. Liu, L. Xu, X. Ma, X. Tan, L. Wu, Q. Qian, T. Wu, J. Zhang, X. Sun and B. Han, Modulating adsorbed hydrogen drives electrochemical CO_2-to-C_2 products, *Nat. Commun.*, 2023, **14**, 4615.

100 J. Zhang, Y. Gu, Y. Lu, C. Zhu, G. Liu, C. Wang, D. Sun, Y. Tang and H. Sun, Each performs its own functions: Nickel oxide supported ruthenium single-atoms and nanoclusters relay catalysis with multi-active sites for efficient alkaline hydrogen evolution reaction, *Appl. Catal., B*, 2023, **325**, 122316.

101 S.-N. Zhao, J.-K. Li, R. Wang, J. Cai and S.-Q. Zang, Electronically and Geometrically Modified Single-Atom Fe Sites by Adjacent Fe Nanoparticles for Enhanced Oxygen Reduction, *Adv. Mater.*, 2022, **34**, 2107291.

102 W. Yang, P. Cheng, Z. Li, Y. Lin, M. Li, J. Zi, H. Shi, G. Li, Z. Lian and H. Li, Tuning the Cobalt–Platinum Alloy Regulating Single-Atom Platinum for Highly Efficient Hydrogen Evolution Reaction, *Adv. Funct. Mater.*, 2022, **32**, 2205920.

103 F. Yu, J. Zhan, D. Chen, J. Guo, S. Zhang and L.-H. Zhang, Electronic States Regulation Induced by the Synergistic Effect of Cu Clusters and Cu-S_1N_3 Sites Boosting Electrocatalytic Performance, *Adv. Funct. Mater.*, 2023, **33**, 2214425.

104 D. Chen, T. Gao, Z. Wei, M. Wang, Y. Ma, D. Xiao, C. Cao, C.-Y. Lee, P. Liu, D. Wang, S. Zhao, H.-T. Wang and L. Han, WS_2 Moiré Superlattices Supporting Au Nanoclusters and Isolated Ru to Boost Hydrogen Production, *Adv. Mater.*, 2024, **36**, 2410537.

105 Y.-K. Lv, Y. Han, K. Wang, W.-Y. Sun, C.-X. Du, R.-W. Huang, P. Peng and S.-Q. Zang, Satellite Pd Single-Atom Embraced AuPd Alloy Nanoclusters for Enhanced Hydrogen Evolution, *ACS Nano*, 2024, **18**, 32186–32195.

106 Y. Li, H. Jiang, L. Lin, Z. Sun and G. Sun, Single-atomic iron synergistic atom-cluster induce remote enhancement toward oxygen reduction reaction, *J. Energy Chem.*, 2025, **102**, 413–420.

107 M. Tang, J. Shen, F. Zhang, Y. Zhao, T. Gan, W. Zeng, R. Li, D. Wang, B. Han and Z. Liu, Upcycling of Polyamide Wastes to Tertiary Amines Using Mo Single Atoms and Rh Nanoparticles, *Angew. Chem., Int. Ed.*, 2025, **64**, e202416436.

108 K. Kong, H. Zhang, A. Han, F. Li and D. Wang, Atomically dispersed metal cocatalysts for solar energy conversion, *Energy Environ. Sci.*, 2024, **17**, 7649–7680.

109 J. Xia, J. Xu, B. Yu, X. Liang, Z. Qiu, H. Li, H. Feng, Y. Li, Y. Cai and H. Wei, A Metal–Sulfur–Carbon Catalyst

Mimicking the Two-Component Architecture of Nitrogenase, *Angew. Chem., Int. Ed.*, 2024, **136**, e202412740.

110 Y. Li, S. Niu, P. Liu, R. Pan, H. Zhang, N. Ahmad, Y. Shi, X. Liang, M. Cheng and S. Chen, Ruthenium Nanoclusters and Single Atoms on α-MoC/N-Doped Carbon Achieves Low-Input/Input-Free Hydrogen Evolution *via* Decoupled/Coupled Hydrazine Oxidation, *Angew. Chem., Int. Ed.*, 2024, **136**, e202316755.

111 R. Liu, Z. Gong, M. Yan, G. Ye and H. Fei, Aligned porous carbon film with ultralow loadings of Pt single atoms and clusters for high-current-density hydrogen generation, *Nano Res.*, 2023, **16**, 256–263.

112 J. Bai, Y. Lian, Y. Deng, M. Xiang, P. Xu, Q. Zhou, Y. Tang and Y. Su, Simultaneous integration of Fe clusters and NiFe dual single atoms in nitrogen-doped carbon for oxygen reduction reaction, *Nano Res.*, 2024, **17**, 2291–2297.

113 M. Ma, Z. Sun, Z. Deng, X. Li, F. Zhang and W. Chen, Synergy enhancement of Co single atoms and asymmetric subnanoclusters for Fenton-like activation, *Nano Res.*, 2024, **17**, 7935–7944.

114 J. Wang, B. Zhang, X. Zheng, X. Liu, W. Guo, Z. Luo, Y. Liu, M. Gao, J. Chen, Z. Zhuang, H. Pan and W. Sun, Pt single atoms coupled with Ru nanoclusters enable robust hydrogen oxidation for high-performance anion exchange membrane fuel cells, *Nano Res.*, 2024, **17**, 6147–6156.